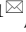
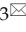



Research Paper

Cancer Theranostic Nanoparticles Self-Assembled from Amphiphilic Small Molecules with Equilibrium Shift-Induced Renal Clearance

Yuan Ma^{1*}, Quanbing Mou^{1*}, Mo Sun¹, Chunyang Yu¹, Jianqi Li², Xiaohua Huang,³ Xinyuan Zhu¹, Deyue Yan¹, and Jian Shen³

1. School of Chemistry and Chemical Engineering, State Key Laboratory of Metal Matrix Composites, Shanghai Jiao Tong University, 800 Dongchuan Road, Shanghai, 200240, P. R. China.
2. Department of Physics and Shanghai Key Laboratory of Functional Magnetic Resonance Imaging, East China Normal University, North Zhongshan Road 3663, Shanghai, 200062, P. R. China.
3. Jiangsu Collaborative Innovation Center of Biomedical Functional Materials, Jiangsu Key Laboratory of Biomedical Materials, College of Chemistry and Materials Science, Nanjing Normal University, Nanjing, 210046, P. R. China.

*Equal contribution.

 Corresponding authors: Xinyuan Zhu, Ph.D., School of Chemistry and Chemical Engineering, State Key Laboratory of Metal Matrix Composites, Shanghai Jiao Tong University, 800 Dongchuan Road, Shanghai, 200240, P. R. China. Jian Shen, Ph.D., Jiangsu Collaborative Innovation Center of Biomedical Functional Materials, Jiangsu Key Laboratory of Biomedical Materials, College of Chemistry and Materials Science, Nanjing Normal University, Nanjing, 210046, P. R. China. E-mail: xy Zhu@sjtu.edu.cn and shenjianshen@hotmail.com

© Ivyspring International Publisher. Reproduction is permitted for personal, noncommercial use, provided that the article is in whole, unmodified, and properly cited. See <http://ivyspring.com/terms> for terms and conditions.

Received: 2016.03.25; Accepted: 2016.05.09; Published: 2016.06.23

Abstract

Nano drug delivery systems have emerged as promising candidates for cancer therapy, whereas their uncertainly complete elimination from the body within specific timescales restricts their clinical translation. Compared with hepatic clearance of nanoparticles, renal excretion of small molecules is preferred to minimize the agent-induced toxicity. Herein, we construct *in vivo* renal-clearable nanoparticles, which are self-assembled from amphiphilic small molecules holding the capabilities of magnetic resonance imaging (MRI) and chemotherapy. The assembled nanoparticles can accumulate in tumor tissues for their nano-characteristics, while the small molecules dismantled from the nanoparticles can be efficiently cleared by kidneys. The renal-clearable nanoparticles exhibit excellent tumor-inhibition performance as well as low side effects and negligible chronic toxicity. These results demonstrate a potential strategy for small molecular nano drug delivery systems with obvious anticancer effect and low-toxic metabolism pathway for clinical applications.

Key words: nanodrug delivery, small molecular nanoparticle, cancer therapy, renal clearance, MRI

Introduction

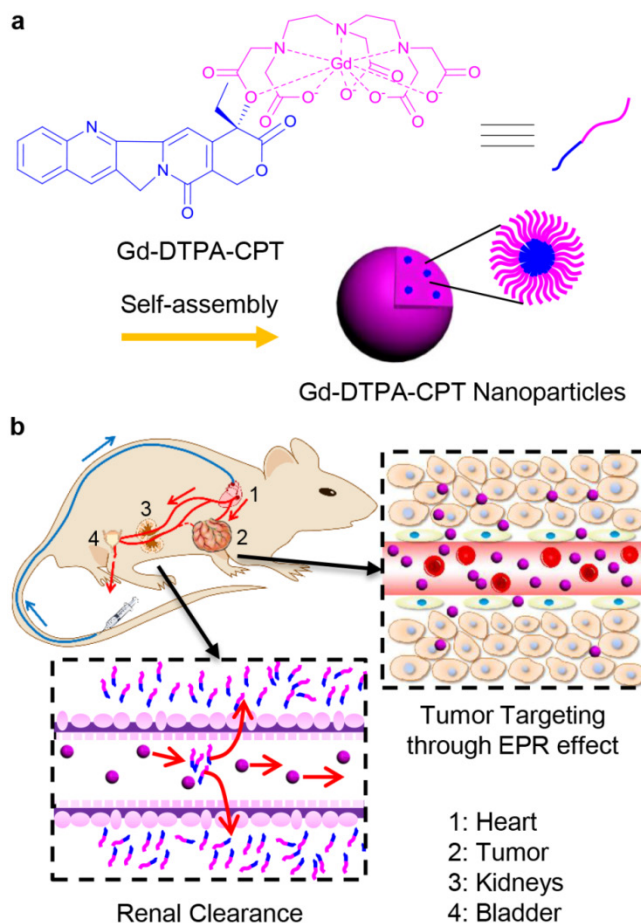
Nanoscale drug delivery systems (DDS) for cancer therapy have become an active research area in recent years.[1] In the past decades, diverse classes of nanoparticle-based delivery vehicles, such as micelles,[2-15] liposomes,[16-18] dendrimers,[19-21] hyperbranched polymers[22-25] and inorganic nanoparticles[26-31] have drawn great attention. Due to the nanoscale property, nanoparticles have prolonged residence time in blood circulation to allow

for preferential tumor accumulation via passive targeting mechanism.[32] However, most nanoparticles severely accumulate in reticuloendothelial system (RES) organs, such as liver and spleen, resulting in poor cancer treatment efficacy.[33] What is even worse, the hepatic processing and biliary excretion are relatively slow, which leads to potential long-term toxicity and tissue damage.[34] Therefore, there is an urgent demand for the development of

nano DDS with negligible organ accumulation and low side effects.

For small molecule anticancer drugs, one efficient strategy for mitigating toxicity is to completely excrete the residual free drugs through rapid renal excretion after therapy.[35,36] Inspired by this fascinating advantage of small molecular metabolism pathway, here we present a facile strategy of nanoparticles self-assembled from amphiphilic small molecules. These nanoparticles exist in rapid equilibrium shift with the small molecules during blood circulation and hence are expected to reveal the properties of both nanoparticles and small molecules. Consequently, the assembled nanoparticles can accumulate in tumors through passive targeting, while the dismantled ones are excreted via the kidneys in the form of free small molecules. To visualize this process in situ, these small molecular nanoparticles are endowed with theranostic function utilizing magnetic resonance imaging (MRI) because of its high spatial resolution and deep tissue penetration.[37-41]

As a proof-of-concept, we designed amphiphilic small molecule consisting of water-soluble MRI contrast agent Gd(DTPA) (DTPA, diethylene triamine pentaacetic acid) and water-insoluble anticancer drug camptothecin (CPT) (Scheme 1a). Gd(DTPA) is one of the most commonly used contrast agents to enhance the tissue contrast of MRI.[42] In addition, CPT is a topoisomerase I (topoI) enzyme inhibitor to induce replication/transcription-mediated DNA damage.[43] The small molecular theranostic nanoparticles are prepared through the aqueous self-assembly of an esterase-responsive amphiphilic molecule Gd(DTPA-CPT), in which Gd(DTPA) is conjugated with CPT through esterification. After injected intravenously, Gd(DTPA-CPT) nanoparticles can accumulate in tumor tissues via passive targeting mechanism (Scheme 1b). Once internalized by cancer cells, Gd(DTPA-CPT) nanoparticles will decompose and release free CPT via ester hydrolysis catalyzed by esterase in the cytoplasm. On the other hand, dissociation of the redundant Gd(DTPA-CPT) nanoparticles in blood circulation would be accelerated because their concentration decreases below the critical aggregation concentration (CAC), resulting in effective clearance from the kidneys and low long-term toxicity. Thanks to the rapid equilibrium shift with small molecules, these nanoparticles would open new avenues for exploration of nano DDS, which integrates with obvious anticancer effect and low-toxic metabolism pathway for clinical applications.



Scheme 1. Gd(DTPA-CPT) nanoparticles for tumor targeting and renal excretion. (a) Schematic illustration of amphiphilic Gd(DTPA-CPT) self-assembly into nanoparticles. (b) Scheme of *in vivo* passive tumor targeting and renal clearance of Gd(DTPA-CPT) nanoparticles.

Experimental Section

Materials

Diethylene triaminepentaacetic acid dianhydride (DTPAA, 98%, TCI), 4-(dimethylamino)pyridine (DMAP, 99%, Aladdin), Gadolinium(III) chloride hexahydrate (99.99%, J&K) were used as received without further purification. CPT (95%) was purchased from Shanghai Knowshine Pharmaceutical Inc. Dulbecco's modified Eagle's medium (DMEM), Ham's F12K medium, fetal bovine serum (FBS), and phosphate-buffered saline (PBS) were purchased from PAA Laboratories GmbH. 3-(4,5-Dimethyl-thiazol-2-yl)-2,5-diphenyl tetrazolium bromide (MTT) was obtained from Sigma-Aldrich. YOYO-1 and Alexa fluor[®] 488 Annexin V/dead cell apoptosis assay kit were purchased from Invitrogen. Ultrapure water was used in all experiments. Clear polystyrene tissue culture treated 6-well, 12-well and 96-well plates were obtained from Corning Costar. All other reagents and

solvents were obtained from the domestic suppliers and used as received.

Measurements

Nuclear magnetic resonance (NMR). ^1H and ^{13}C NMR spectra were recorded on Bruker AVANCEIII 400 spectrometer with dimethylsulfoxide- d_6 (DMSO- d_6) as a solvent (^1H at 400 MHz, ^{13}C at 100 MHz).

Mass spectrometry (MS). MS experiments were carried out on a Waters Q-TOF Premier Mass Spectrometer, employing electrospray ionization in negative mode.

Ultraviolet-visible absorption (UV-vis). UV-vis absorption of the sample solutions was measured by using a Thermo Electron-EV300 UV-vis spectrophotometer at room temperature. The slit-width was set as 1 nm with a scan speed of 480 nm min^{-1} .

Fluorescent spectra. The fluorescent spectra were performed on QC-4-CW spectrometer, provided by Photon Technology International, Int. USA/CAN. The voltage was set as 13.4 V, and the slit-width was set as 4 nm. The excitation wavelength was set as 359 nm (the maximum intensity obtained in the excitation spectra). The step increment was set as 2 nm, and scan speed was set as 480 nm min^{-1} .

Fourier transform infrared spectra (FTIR). FTIR spectra were recorded on a Paragon 1,000 instrument by KBr sample holder method.

Dynamic light scattering (DLS). DLS measurements were performed by a Zetasizer Nano ZS90 (Malvern Instruments Ltd.) equipped with a 125 mW laser at 25 °C. The scattering angle was kept at 173° and the wavelength was set as 633 nm during the whole experiment.

Transmission electron microscopy (TEM). TEM studies of Gd(DTPA-CPT) nanoparticles were performed on a JEOL 2010 microscope at an accelerating voltage of 200 kV. A little drop of solution containing Gd(DTPA-CPT) nanoparticles (0.2 mg mL^{-1}) was spread onto a carbon-coated copper grid and stabilized with carbon film coating. Then, the sample was lyophilized by a freeze-dryer (Christ Alpha 1-4 LD plus, Germany) before measurement.

Methods

Synthesis of DTPA-CPT

DTPAA (2.142 g, 6 mmol) and DMAP (0.122 g, 1 mmol) were dissolved in dried DMSO (30 mL), and the mixture was stirred at 0 °C for 30 min. Then the mixture was added to a solution of CPT (0.348 g, 1 mmol) and dried DMSO (35 mL). The resulting solution was stirred at room temperature for 2 days in the dark under nitrogen protection. Then the reaction

solution was concentrated under vacuum. The crude product was purified by Preparative Chromatography (Lisure Inc.) with a C18 reversed phase column. The mobile phase consisted of acetonitrile and water. The detection wavelength was set as 254 nm. The solvent was removed by rotary evaporation and the yellowy solid product was collected (0.441 g, 61% yield). ^1H NMR (400 MHz, DMSO- d_6 , δ): 8.67 (s, 1H), 8.16 (d, $J = 8.5$ Hz, 1H), 8.11 (d, $J = 8.0$ Hz, 1H), 7.84 (t, $J = 7.7$ Hz, 1H), 7.70 (t, $J = 8.0$ Hz, 1H), 7.11 (s, 1H), 5.49 (s, 2H), 5.28 (s, 2H), 3.88 (d, $J = 17.7$ Hz, 1H), 3.78 (d, $J = 17.7$ Hz, 1H), 3.45-3.43 (m, 8H), 2.91-2.77 (m, 8H), 2.18-2.08 (m, 2H), 0.91 (t, $J = 7.4$ Hz, 3H); ^{13}C NMR (100 MHz, DMSO- d_6 , δ): 172.58, 170.54, 169.90, 167.39, 156.64, 152.42, 147.97, 146.13, 145.44, 131.63, 130.48, 129.86, 129.06, 128.58, 128.06, 127.78, 118.81, 95.07, 76.33, 66.39, 54.97, 54.85, 54.71, 54.33, 51.70, 50.31, 50.03, 30.30, 7.72; HRMS (ESI) m/z : [M-H] $^-$ calcd. for $\text{C}_{34}\text{H}_{36}\text{N}_5\text{O}_{13}$, 722.2310; found, 722.2307.

Gadolinium(III) chelation to DTPA-CPT

The ligand DTPA-CPT (0.145 g, 0.2 mmol) was dispersed in deionized water (10.0 mL) and the pH was adjusted to 5.5-6.5 with dilute sodium hydroxide (NaOH) solution. After DTPA-CPT dissolved completely, the aqueous solution of GdCl_3 (52.8 mg, 0.2 mmol) was then added to the above solution and stirred at room temperature for 8 h. Then the reaction mixture was dialyzed using dialysis membranes of 3 kDa molecular weight cutoff for 2 days against ultrapure water to remove free Gd^{3+} . Purified Gd(DTPA-CPT) was obtained by freeze-drying. Gd chelation was confirmed by FTIR analysis. Gd content in Gd(DTPA-CPT) was determined by an inductively coupled plasma-atomic emission spectrometer (ICP-AES, Spectro Genesis).

Preparation and characterization of Gd(DTPA-CPT) nanoparticles

1.0 mg Gd(DTPA-CPT) was dissolved in ultrapure water (1.0 mL) in a round-bottomed flask. Subsequently, the solution was evaporated and dried on vacuum for 8 h. Then, 1.0 mL of ultrapure water was added to the flask and successively placed in a bath sonicator for 30 min, which is helpful to achieve well distributed nanoparticles.

Preparation of Nile-red loaded Gd(DTPA-CPT) nanoparticles

1.0 mg Gd(DTPA-CPT) and predetermined amount of Nile-red were dissolved in DMSO and mixed well at room temperature. Subsequently, 1.0 mL of deionized water was added into the DMSO solution drop by drop in 30 min. Then the mixture

was dialyzed against deionized water for 24 h (Mw cutoff: 500 Da) at room temperature and the deionized water was renewed every 3 h. The final concentration of Gd(DTPA-CPT) was measured by the absorbance at 356 nm by UV-vis spectrophotometer, wherein calibration curve was obtained with serial concentrations of Gd(DTPA-CPT).

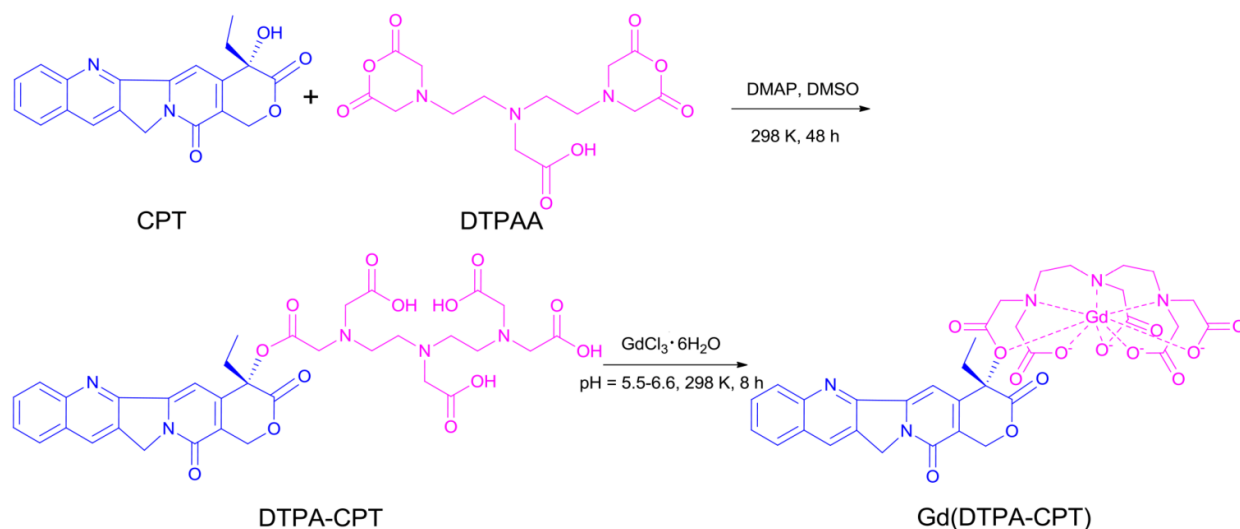
Synthesis of pyrene-labeled block copolymer poly(ethylene glycol)-block-poly(caprolactone) (PEG-*b*-PCL)

PEG-*b*-PCL was synthesized according to the literature.[44] 1-Pyrenebutanoic acid (0.288 g, 1 mmol) and DCC (0.206 g, 1 mmol) were dissolved in dried CH₂Cl₂ (25.0 mL), and the mixture was stirred at 0 °C. After 30 min, the mixture was added to a solution of PEG-*b*-PCL (5.000 g, 1 mmol, M_n = 3.7 × 10³), DMAP (0.061 g, 0.5 mmol) and CH₂Cl₂ (25.0 mL), then the resulting solution was stirred for 24 h at room temperature in the dark. After the reaction was completed, the mixture was filtered to remove dicyclohexylurea (DCU) and the filtrate was concentrated under vacuum to get crude product. The raw product was further purified by precipitation into ethyl ether. The product was collected and the solvent was removed by rotary evaporation to give a white solid (4.417 g, 84%).

Results and discussion

To prepare the small molecular nanoparticles, amphiphilic Gd(DTPA-CPT) conjugate was designed and synthesized as shown in Scheme 2. DTPA-CPT

was obtained via esterification of DTPAA and CPT using DMAP as a catalyst. The reaction proceeded well to afford the desired product DTPA-CPT in moderate to good yields. The side reaction for DTPA-CPT₂ (Figure S1) could be negligible, probably due to the steric hindrance effect and low reactivity of the hydroxyl of CPT. The chemical structure of DTPA-CPT was validated by ¹H nuclear magnetic resonance spectroscopy (¹H NMR) and ¹³C NMR (Figure S2 and S3). As shown in Figure 1a, compared with the ¹H NMR spectrum of CPT, the peak at 6.55 ppm (1) belonging to hydroxyl proton of CPT disappears completely. Furthermore, the two proton signals at 1.88 ppm (2) related to the methylene (CH₃CH₂-, lactonic ring) of CPT shift to 2.14 ppm (2'). These results suggest that the esterification reaction has occurred. In addition, the high resolution mass spectroscopy (HRMS) confirms that the molecular weight of DTPA-CPT (m/z, [M-H]⁻) is 722.2307 (Figure S4), which agrees with the calculated value 722.2310 (m/z, [M-H]⁻) very well. Subsequently, DTPA-CPT ligand was reacted with GdCl₃ at room temperature for 8 h to get Gd(DTPA-CPT). The identities of DTPA-CPT and Gd(DTPA-CPT) were further confirmed by FTIR, UV-vis, and fluorescence spectroscopy (Figures S5-S7). As determined by ICP-AES, the Gd content of Gd(DTPA-CPT) was 17.2%, which is in agreement with the calculated value (17.9%). All experimental results demonstrate that Gd(DTPA-CPT) was synthesized successfully.



Scheme 2. The synthesis route of Gd(DTPA-CPT).

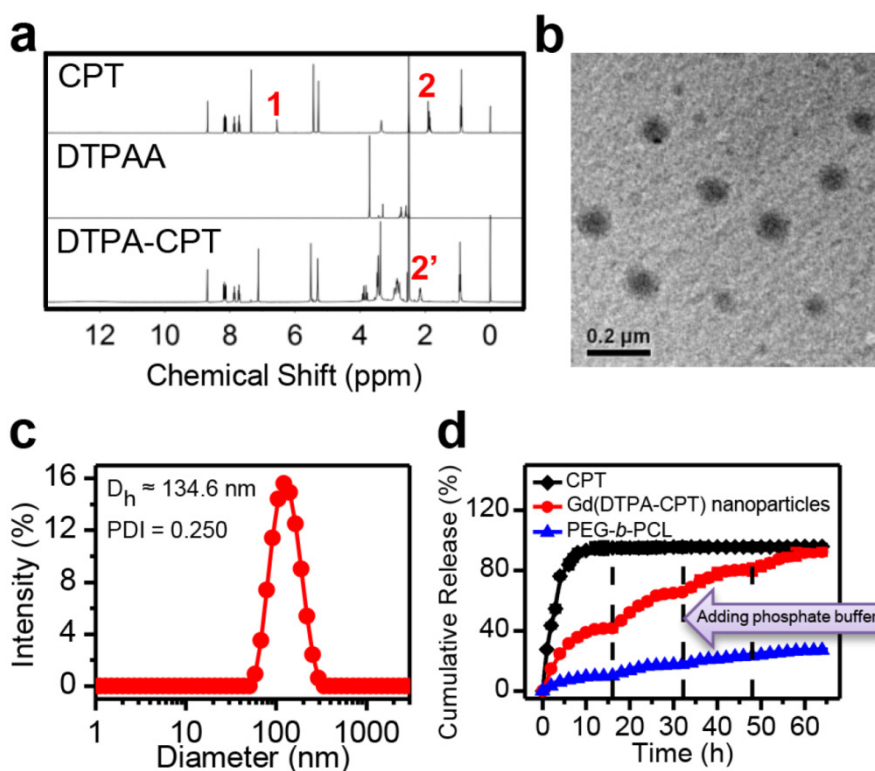


Figure 1. Characterization of Gd(DTPA-CPT) nanoparticles. (a) ¹H NMR spectra of CPT, DTPAA, and DTPA-CPT in DMSO-*d*₆. (b) Representative TEM image of Gd(DTPA-CPT) nanoparticles. Scale bar, 0.2 μm. (c) Hydrodynamic diameter distribution of Gd(DTPA-CPT) nanoparticles in water. (d) Diffusion rate of free CPT, Gd(DTPA-CPT) nanoparticles and PEG-*b*-PCL nanoparticles determined by equilibrium dialysis.

Due to its inherent amphiphilicity, Gd(DTPA-CPT) self-assembled into nanoparticles in aqueous solution. The nanoparticles could be dispersed in water without aggregation after one week storage. The TEM images reveal the presence of spherical nanoparticles with an average diameter of ~95.4 nm (Figure 1b). According to the DLS studies, the intensity-average hydrodynamic diameter (D_h) is approximate 134.6 nm (Figure 1c). To evaluate the aggregation behavior of Gd(DTPA-CPT) in aqueous solution, the CAC was measured by fluorescence spectroscopy using pyrene as a hydrophobic fluorescent probe. Pyrene preferentially partitions into the hydrophobic nanoparticle core, causing changes in photophysical properties.[45] According to the inflection of the curve in Figure S14, the CAC value of Gd(DTPA-CPT) is 7.1 μg mL⁻¹. As is well known, small molecular-based nanoparticles have higher CAC value than polymeric nanoparticles, which is a very critical indicator for nanoparticle stability.[33] Hence, small molecular-based nanoparticles may exhibit obvious dynamic equilibrium properties, which is different from polymeric nanoparticles. To compare the equilibrium properties, the relative stability of Gd(DTPA-CPT) and pyrene-labeled PEG-*b*-PCL nanoparticles was investigated by using molecular dynamics simulations. The details of the simulation model and

method are described in the Supporting Information. The average binding energy (E_b) of one Gd(DTPA-CPT) and PEG-*b*-PCL molecule in nanoparticles is defined as:

$$E_b = [E(\text{nanoparticle}) - n \times E(\text{monomer})] / n \quad \dots(1)$$

where $E(\text{nanoparticle})$ is the total potential energy of Gd(DTPA-CPT) or PEG-*b*-PCL nanoparticle, $E(\text{monomer})$ is the energy of Gd(DTPA-CPT) or PEG-*b*-PCL monomer and n is the number of Gd(DTPA-CPT) or PEG-*b*-PCL. As shown in Table 1, the calculated average binding energy of Gd(DTPA-CPT) is much higher than that of PEG-*b*-PCL, which indicates that free Gd(DTPA-CPT) has more opportunity to escape from the nanoparticles to induce the equilibrium shift between small molecules and nanoparticles.

To further verify the equilibrium shift of Gd(DTPA-CPT) nanoparticles, equilibrium dialysis was performed using dialysis membranes of 10 kDa molecular weight cutoff, employing free CPT and PEG-*b*-PCL nanoparticles as controls. In addition, to mimic the dilution by plasma administration, determined amounts of phosphate buffer (pH 7.4) were added outside the dialysis bag at different time intervals. Due to the small nominal pore size of the dialysis membrane, only free CPT and Gd(DTPA-CPT), as well as unimer of PEG-*b*-PCL can

diffuse through the dialysis membranes. As shown in Figure 1d, the rapid diffusion of free CPT out of the dialysis membranes was observed within 16 h. Compared with free CPT, the diffusion of Gd(DTPA-CPT) nanoparticles is much slower, which can be ascribed to the slow dissociation of Gd(DTPA-CPT) nanoparticles. When the equilibrium was achieved, determined amount of phosphate buffer was added outside the dialysis bag to broke the balance and trigger another cycle of dissociation of nanoparticles. Disturbed by the dilution process, the equilibrium between nanoparticles and small molecules starts to shift towards small molecules, which causes nanoparticles to disassemble and permits drug diffusion out of the dialysis bag. Furthermore, multiple dilution processes could be performed until nearly all Gd(DTPA-CPT) pass through the dialysis membranes. On the other hand, for polymeric nanoparticles, relatively small amount of PEG-*b*-PCL unimer is detected out of the dialysis membranes due to its high stability. From the aforementioned results, it can be concluded that Gd(DTPA-CPT) nanoparticles exist in equilibrium with small molecules, and are less stable than polymeric nanoparticles. Once the equilibrium is shifted towards small molecule, the dissociation of Gd(DTPA-CPT) nanoparticles is facilitated to release small molecule.

Table 1. Calculated binding energies by using molecular dynamics simulations.

Sample	Aggregation number	E_b (kJ/mol)
Gd(DTPA-CPT)	25	-168.17
	50	-206.55
PEG- <i>b</i> -PCL	25	-1044.78
	50	-1112.40

Controlled and sustained release of drug from nanoparticles is important for cancer therapy. CPT is expected to be released from Gd(DTPA-CPT) nanoparticles upon hydrolysis of the ester bond in tumor cells. To evaluate the *in vitro* drug release kinetics, Gd(DTPA-CPT) nanoparticles were incubated at 37 °C in different environments to mimic various physiological conditions (phosphate buffer (pH 7.4), acetate buffer (pH 5.0), phosphate buffer (pH 7.4) containing 17 U mL⁻¹ esterase and acetate buffer (pH 5.0) containing 17 U mL⁻¹ esterase). The release of CPT from Gd(DTPA-CPT) nanoparticles was determined using HPLC. As illustrated in Figure S17, Gd(DTPA-CPT) nanoparticles slowly hydrolyze and release CPT at neutral pH, which suggests low drug leakage during blood circulation. However, hydrolysis is accelerated with more and more free

CPT released in a weakly acidic environment (pH 5.0). In the presence of esterase, which is abundant in cytoplasm,[46] Gd(DTPA-CPT) nanoparticles quickly hydrolyze and release free CPT. Therefore, Gd(DTPA-CPT) nanoparticles can be used as prodrug for intracellular release of CPT.

Considering the strong blue fluorescence emitted by Gd(DTPA-CPT), the ability of these nanoparticles to enter cancer cells was studied by CLSM. The LoVo cells were incubated with Ham's F12K medium containing Gd(DTPA-CPT) nanoparticles at a concentration of 30 μM at 37 °C for 3 h before observation. The nuclei were stained with DNA fluorescent intercalator dye YOYO-1 for 20 min before observation. As shown in Figure 2a, the blue emission of Gd(DTPA-CPT) is observed within the cytoplasm and nuclei, which suggests that Gd(DTPA-CPT) nanoparticles can be internalized by cancer cells. To gain insight into the cell uptake velocity, flow cytometry analysis was performed to measure the intracellular fluorescence intensity of Gd(DTPA-CPT) nanoparticles using Nile red as a fluorescent probe. As shown in Figure 2b and c, the mean fluorescence intensity of cells increases with the incubation time, which indicates that Gd(DTPA-CPT) nanoparticles are internalized by LoVo cells.

In vitro anticancer efficacy of Gd(DTPA-CPT) nanoparticles was evaluated against LoVo and HepG2 cells using MTT assay, employing CPT, Gd(DTPA) and Gd(DTPA)/CPT mixture as controls. As illustrated in Figure 3a, b and Figure S18, S19, Gd(DTPA-CPT) nanoparticles show the same cytotoxicity as free CPT and Gd(DTPA)/CPT mixture against both of the cell lines. After 48 h incubation, the IC₅₀ values of Gd(DTPA-CPT) nanoparticles are 1.71 μM for Lovo cells and 0.53 μM for HepG2 cells, respectively (Table S2 and S3). From these results, it is clearly confirmed that Gd(DTPA-CPT) nanoparticles exhibit significant *in vitro* anticancer activity. On the other hand, Gd(DTPA) shows no obvious cytotoxicity even at high concentrations against the LoVo and HepG2 cells.

Furthermore, the apoptosis of LoVo cells induced by free CPT, Gd(DTPA), Gd(DTPA-CPT) and Gd(DTPA)/CPT mixture was confirmed by FITC-Annexin V/PI flow cytometry assay. LoVo cells were cultured with free CPT, Gd(DTPA), Gd(DTPA-CPT) and Gd(DTPA)/CPT mixture at a concentration of 3 μM for 24 h, respectively. The untreated LoVo cells were used as controls. As shown in Figure 3c, the Gd(DTPA) treated cells don't show any significant apoptosis or necrosis. In addition, Gd(DTPA-CPT) prompts a large population of cells to undergo early (29.9%) and late (14.2%) stage apoptosis, which is similar to the free CPT (24.5%

early apoptosis and 20.9% late apoptosis) and Gd(DTPA)/CPT mixture (24.3% early apoptosis and 22.6% late apoptosis) treated groups. The results demonstrate that Gd(DTPA-CPT) exhibits remarkable ability to induce cell apoptosis.

To evaluate the hemocompatibility of Gd-DTPA-CPT, the *in vitro* hemolysis assay was also conducted by testing the amount of the hemoglobin released from red blood cells (RBC) under physiological conditions, using polyethylenimine

(PEI) and dextran as reference, and Triton X-100 as 100% hemolysis value. As shown in Figure S20, Gd-DTPA-CPT induce negligible hemoglobin release, which is comparable to dextran, and significantly lower than the corresponding value of PEI. Hence, Gd-DTPA-CPT exhibits negligible hemolytic activity. These *in vitro* evaluations confirm that Gd-DTPA-CPT exhibit good biocompatibility and may be administered via tail vein injection.

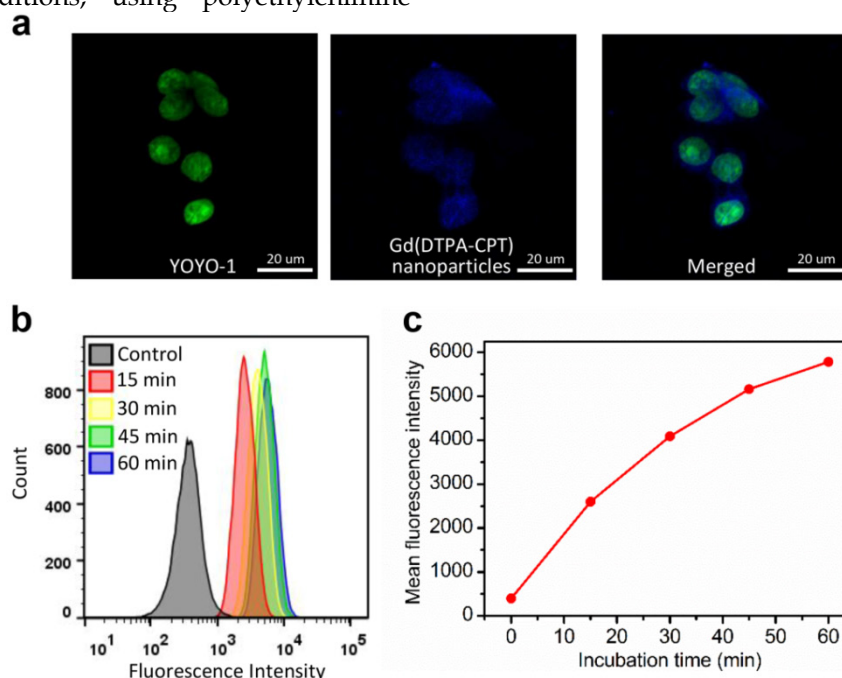


Figure 2. Cellular uptake of Gd(DTPA-CPT) nanoparticles by LoVo cells. (a) CLSM images of LoVo cells incubated with Gd(DTPA-CPT) nanoparticles (blue) for 3 h. Cell nuclei (green) were stained with YOYO-1. Scale bar, 20 μm. (b) Flow cytometric profiles of LoVo cells incubated with Gd(DTPA-CPT) nanoparticles at different time intervals. (c) Time-dependent profiles of mean fluorescence intensity in LoVo cells determined by flow cytometry analysis.

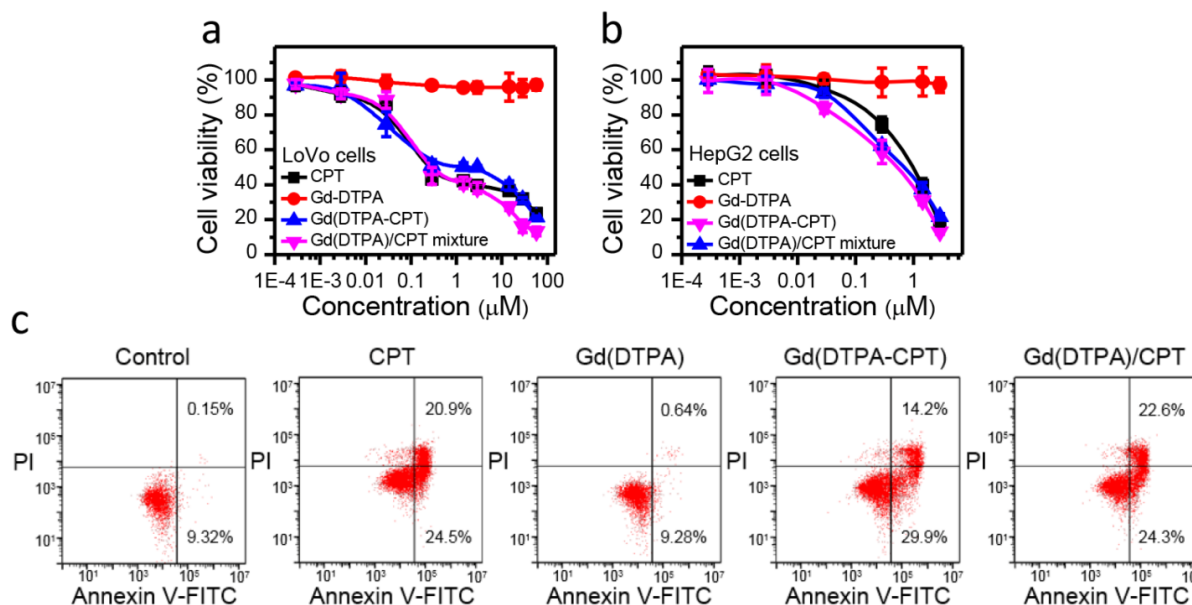


Figure 3. Effect of Gd(DTPA-CPT) nanoparticles on cancer cell growth and apoptosis. (a,b) Cell viability assay of CPT, Gd(DTPA), Gd(DTPA-CPT) nanoparticles and Gd(DTPA)/CPT mixture to LoVo (a) and HepG2 (b) cell lines determined by MTT assay, respectively. (c) Induction of apoptosis by CPT, Gd(DTPA), Gd(DTPA-CPT) nanoparticles and Gd(DTPA)/CPT mixture in LoVo cells as determined by FITC-Annexin V/PI flow cytometry assay. The lower left quadrant, viable and non-apoptotic cells; the lower right quadrant, early apoptotic cells; the upper right quadrant, late apoptotic cells; the upper left quadrant, necrotic cells. The numbers in the quadrants represent the percentage of early or late apoptotic cells.

To investigate the MRI relaxivity of Gd(DTPA-CPT) nanoparticles, typical T_1 -weighted spin-echo MR images recorded for Gd(DTPA-CPT) nanoparticles in aqueous solution were measured by a clinical 3 T Siemens Magnetom Trio Tim (Figure 4a). Gd(DTPA), clinically used T_1 -type contrast agent, was examined as a reference. Upon gradual increase of Gd concentration, positive contrast enhancement was observed, as revealed by the elevated brightness. As illustrated in Figure 4b, quantitative analysis of the results reveals an almost linear relationship between water proton longitudinal relaxation rate ($1/T_1$) and Gd concentrations. The T_1 relaxivity (r_1) of Gd(DTPA-CPT) nanoparticles is calculated to be $4.66 \text{ mM}^{-1} \text{ s}^{-1}$, slightly higher than that of Gd(DTPA) ($4.05 \text{ mM}^{-1} \text{ s}^{-1}$), which can be interpreted by the theory for MRI contrast agent (see Supporting Information). These results suggest that, the Gd(DTPA-CPT) nanoparticles can serve as T_1 -type MRI contrast agent to monitor the drug delivery behavior.

As one of the most powerful imaging techniques, MRI imparts deep penetration into soft tissues with high spatiotemporal resolution and imaging sensitivity, making it the optimal method for theranostics.[47-52] Therefore, the tumor accumulation and biodistribution of Gd(DTPA-CPT) nanoparticles were investigated by MRI experiments recorded for nude mice bearing LoVo tumors, employing Gd(DTPA) as a control. As shown in

Figure 5a, Gd(DTPA-CPT) nanoparticles treated group shows significantly positive contrast enhancement in tumors in comparison of pre- and postcontrast MR images. Moreover, the signal enhancement is persistent within 5 h post-administration. In contrast, no discernible changes of MRI signals in Gd(DTPA) treated group can be observed (Figure 5b). The prominent accumulation might be ascribed to the passive targeting effect. Moreover, the significant contrast enhancement in kidneys (Figure 5c) suggests that Gd(DTPA-CPT) is excreted through kidney via glomerular filtration. Gradual enhancement in the urinary bladder is also observed, indicating urinary clearance of Gd(DTPA-CPT) (Figure S21). It is notable that the renal excretion of Gd(DTPA-CPT) is slower than that of Gd(DTPA), which reveals the nano-scale characteristics of nanoparticles (Figure 5d). The aforementioned results indicate that, a portion of Gd(DTPA-CPT) nanoparticles could accumulate in the tumor tissue through the “enhanced permeability and retention” (EPR) effect.[32] After carrying out their biological function, the remaining nanoparticles undergo a reduction in concentration during blood circulation. Thus, Gd(DTPA-CPT) nanoparticles are dismantled into small molecules and subsequently excreted through kidney. This route of renal clearance is clinically preferable because it is much faster and safer than hepatobiliary route.[34,53,54]

To further investigate the retention time of Gd(DTPA-CPT) nanoparticles, the blood elimination profiles of Gd(DTPA-CPT) nanoparticles and Gd(DTPA) after intravenous injection are presented in Figure 6a. SD rats were intravenously injected with Gd(DTPA-CPT) nanoparticles or free Gd(DTPA) ($0.10 \text{ mmol kg}^{-1}$), respectively. Overall, both formulations display fast clearance from the blood circulation within the first 2.5 h, which implies the distribution of drug into tissues. Compared with free Gd(DTPA), Gd(DTPA-CPT) has slightly longer blood retention time, which may be ascribed to nano-characteristics of nanoparticles. Furthermore, to assess the tumor targeting efficacy and renal excretion, the biodistribution of Gd(DTPA-CPT) nanoparticles in organs and tumors were studied. The LoVo tumor-bearing mice were sacrificed at 0.5 h, 5 h and 18 h post-administration, respectively. The biodistribution profiles of Gd(DTPA-CPT) nanoparticles were compared with Gd(DTPA) by analyzing the residual Gd

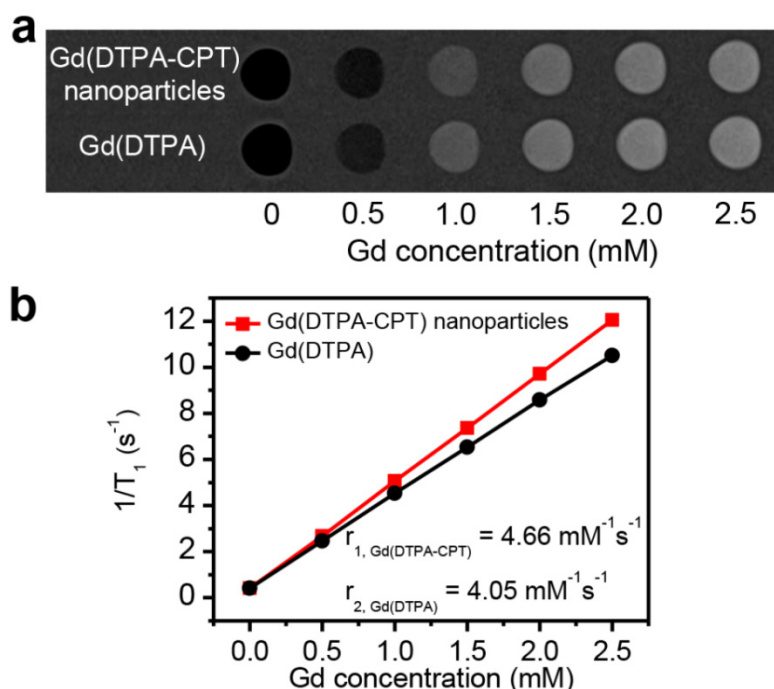


Figure 4. *In vitro* MRI relaxivity of Gd(DTPA-CPT) nanoparticles. (a) T_1 -weighted spin-echo MR images recorded for aqueous solutions of Gd(DTPA-CPT) nanoparticles. (b) Water proton longitudinal relaxation rate ($1/T_1$) of Gd(DTPA-CPT) nanoparticles in aqueous solution as a function of Gd concentration.

by ICP-MS. As shown in Figure 6b, the accumulation in heart, lung and spleen is relatively similar between Gd(DTPA-CPT) nanoparticles and Gd(DTPA). In contrast, in the mice treated with Gd(DTPA-CPT) nanoparticles, the liver uptake is higher than Gd(DTPA) treated group, which reveals difference between nanoparticles and small molecules. In addition, unlike most polymeric nanoparticles which severely accumulate in the RES organs,[55-57] the highest amount of Gd is detected in kidneys from Gd(DTPA-CPT) nanoparticle treated group. These results demonstrate that Gd(DTPA-CPT) undergo renal clearance *in vivo*. Considering the kidney

filtration threshold (KFT, 5.5 nm), Gd(DTPA-CPT) nanoparticles should disassemble into small molecules to undergo renal clearance. Specifically, Gd(DTPA-CPT) nanoparticles preferentially accumulate in solid tumors as compared with free Gd(DTPA), which is ascribed to the passive targeting mechanism (Figure 6b). These results indicate that the Gd(DTPA-CPT) nanoparticles could accumulate in tumor through passive targeting effect. Meanwhile, when the concentration is below CAC, they disintegrate into small molecules and are excreted through kidneys subsequently.

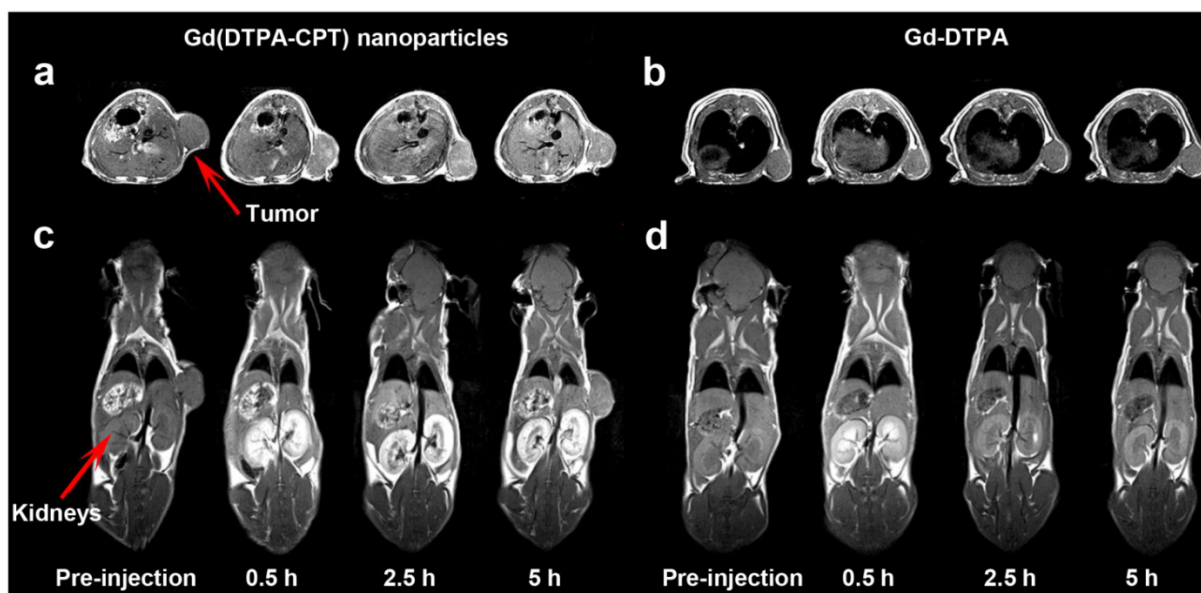


Figure 5. *In vivo* T₁-weighted MR images of nude mice bearing LoVo tumors at pre-injection and 0.5, 2.5, 5 h after intravenous injection of Gd(DTPA-CPT) nanoparticles and Gd(DTPA) at a dose of 0.10 mmol kg⁻¹. a,b) The transverse T₁-weighted MR images of mice before and after treated with Gd(DTPA-CPT) nanoparticles (a) and Gd(DTPA) (b). c,d) Representative coronal T₁-weighted MR images of nude mice before and after injected with Gd(DTPA-CPT) nanoparticles (c) and Gd(DTPA) (d). (Note: In **Figure 5a,c**, the tumor positions were different, which was due to the shift of subcutaneous tumors. At different time intervals before scanning, the anesthetized mouse was put into the coil and wrapped by gauze to avoid death from cold. The gauze squeezed the tumor and then shift it to different positions.)

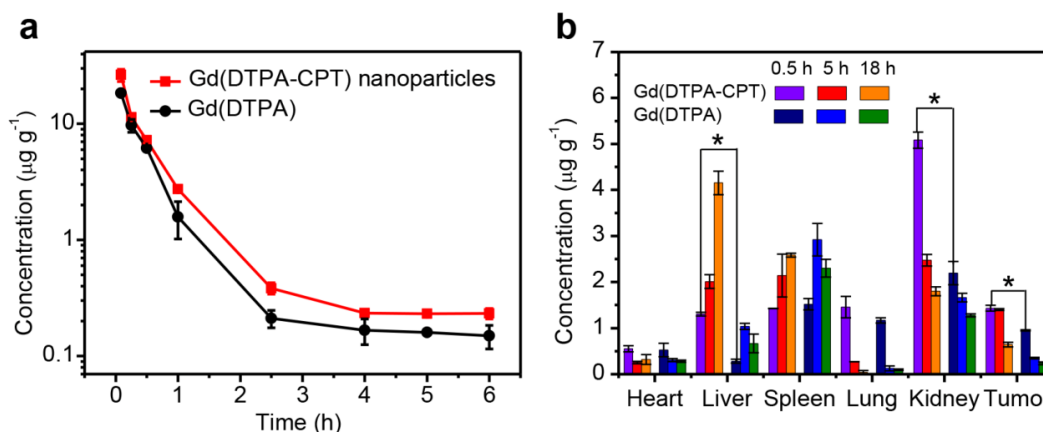


Figure 6. *In vivo* pharmacokinetics and biodistribution studies of Gd(DTPA-CPT) nanoparticles. (a) Blood elimination profiles of Gd(DTPA-CPT) nanoparticles and Gd(DTPA) following a single intravenous injection into rats at a dose of 0.10 mmol kg⁻¹. Data represent mean \pm SD (n = 4). (b) Biodistribution of Gd(DTPA-CPT) nanoparticles and Gd(DTPA) in various tissues after 0.5 h, 5 h and 18 h post-injection (0.10 mmol kg⁻¹) into nude mice bearing LoVo tumors. Data represent mean \pm SD (n = 4). Statistical significance: *, P < 0.05.

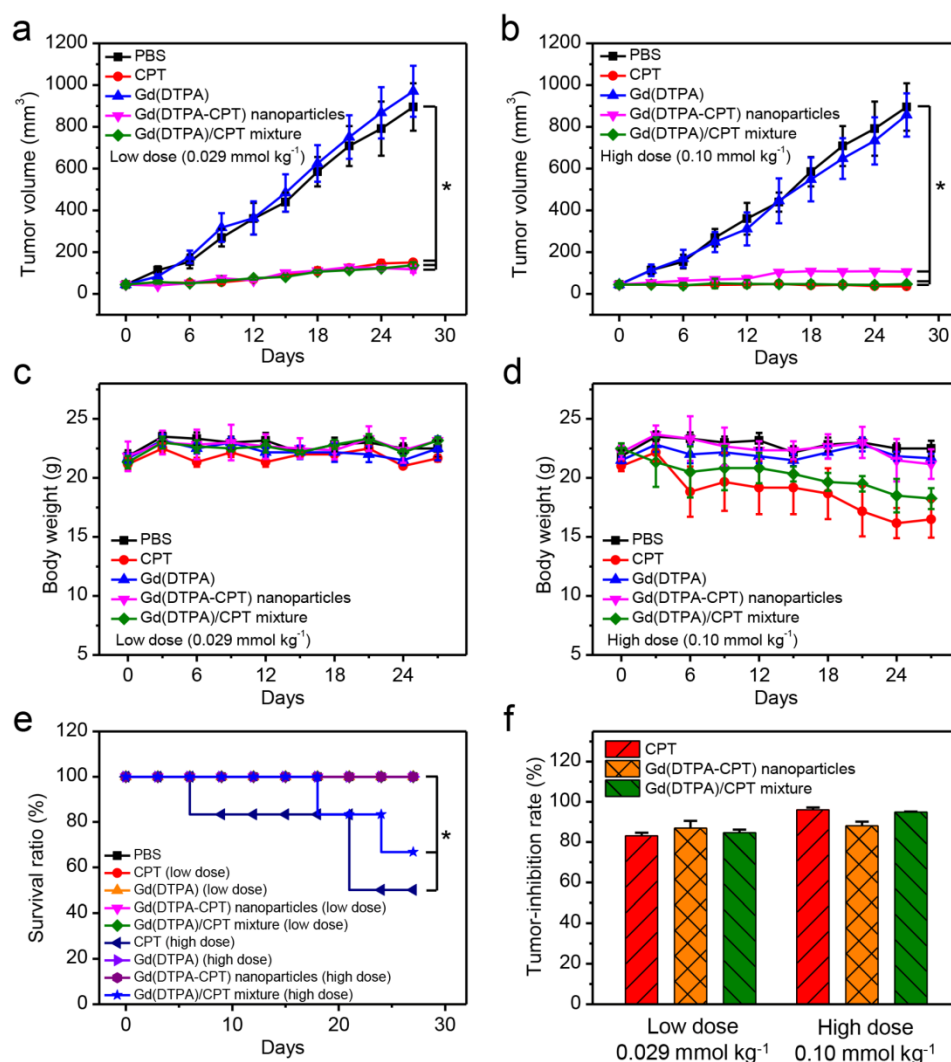


Figure 7. *In vivo* anticancer activities of PBS, CPT, Gd(DTPA), Gd(DTPA-CPT) nanoparticles and Gd(DTPA)/CPT mixture i.v. administered at doses of 0.029 and 0.10 mmol kg⁻¹, respectively, against nude mice bearing LoVo xenograft tumors (n = 6, data expressed as average ± s.d.). Statistical significance: *, P < 0.05. (a,b) The tumor volumes of mice bearing LoVo tumors exposed to various formulations. The mice in different treatment groups were intravenously injected via the tail vein with PBS, CPT, Gd(DTPA), Gd(DTPA-CPT) nanoparticles and Gd(DTPA)/CPT mixture at doses of 0.029 mmol kg⁻¹ (low dose) (a) or 0.10 mmol kg⁻¹ (high dose) (b) once every 3 days, respectively. (c,d) The body weight changes of mice after different treatments at doses of 0.029 mmol kg⁻¹ (low dose) (c) or 0.10 mmol kg⁻¹ (high dose) (d). (e) Survival curves of each group of the mice. (f) The tumor inhibitory rates (TIR) after different treatments. The TIR is calculated using the following equation: $TIR = 100\% \times (V_c - V_t) / V_c$, where V_c and V_t are the mean tumor volumes of the control and the treated mice, respectively.

The *in vivo* antitumor activities were investigated using mice bearing LoVo tumors. The mice were divided into five groups (n = 6) randomly. Typically, the recommended injection dose for MR imaging is 0.10 mmol kg⁻¹, and the appropriate therapeutic dose of CPT is 0.029 mmol kg⁻¹. [58] Therefore, the mice in different treatment groups were intravenously injected via the tail vein with PBS, CPT, Gd(DTPA), Gd(DTPA-CPT) nanoparticles and Gd(DTPA)/CPT mixture at doses of 0.029 mmol kg⁻¹ (low dose) or 0.10 mmol kg⁻¹ (high dose) once every 3 days, respectively. As shown in Figure 7a, 7b and Figure S22, tumor growths are remarkably suppressed by the treatment of Gd(DTPA-CPT) nanoparticles, free CPT and Gd(DTPA)/CPT mixture compared with the control group (PBS). The tumor inhibitory rates (TIR) of

low-dose treated group on LoVo tumors were 83.1% (CPT), 86.9% (Gd(DTPA-CPT)), 84.6% (Gd(DTPA)/CPT mixture) (Figure 7f). For high-dose treated group, the TIR were 96.0% (CPT), 88.1% (Gd(DTPA-CPT)), 94.8% (Gd(DTPA)/CPT mixture) respectively. Remarkably, Gd(DTPA-CPT) nanoparticles exhibit significant tumor inhibition efficacy in mice bearing LoVo tumors at both doses. The body weights of mice treated with different formulations were also examined (Figure 7c and d). No acute body weight drop is observed for Gd(DTPA-CPT) nanoparticle treated groups at different doses, suggesting no severe toxicity for Gd(DTPA-CPT) nanoparticles. However, in CPT and Gd(DTPA)/CPT mixture (high dose) treated group, acute body weight drop is observed. As shown in

Figure 7e, the survival rates of mice in different groups were also recorded. No treatment related deaths are reported in Gd(DTPA-CPT) nanoparticle treated groups at different doses. However, the mice treated with CPT and Gd(DTPA)/CPT mixture (high dose) show 50% and 63.7% survival rate at the end of experiment, respectively. It can be deduced that free CPT presents severer systemic toxicity compared with Gd(DTPA-CPT) nanoparticles. Therefore, Gd(DTPA-CPT) nanoparticles remarkably suppress the tumor growth and show no obvious toxicity, whereas free CPT could lead to serious toxicity in mice. Hence, Gd(DTPA-CPT) nanoparticles are hopeful to achieve the same therapeutic effect as well as lower side effects than free CPT.

To assess the antitumor activities after treatments with various formulations, the excised

tumor tissues were also fixed and prepared for H&E staining. In the PBS control group, the tumor tissue is constructed by tightly packed LoVo cells interspersed with stroma, with rarely observed apoptotic tumor cells. After administration with Gd(DTPA-CPT) nanoparticles or CPT, significant differences are observed in the histological features of tumors compared with the PBS control group (Figure 8a). For example, in groups treated with Gd(DTPA-CPT) nanoparticles or free CPT, the tumor cellularity reduces significantly compared with the PBS control group. Besides, many cancer cells are composed of membrane-bound, nuclear shrinkage and small nuclear fragments surrounded by a rim of cytoplasm, which implies the occurrence of vacuolization and typical apoptosis.

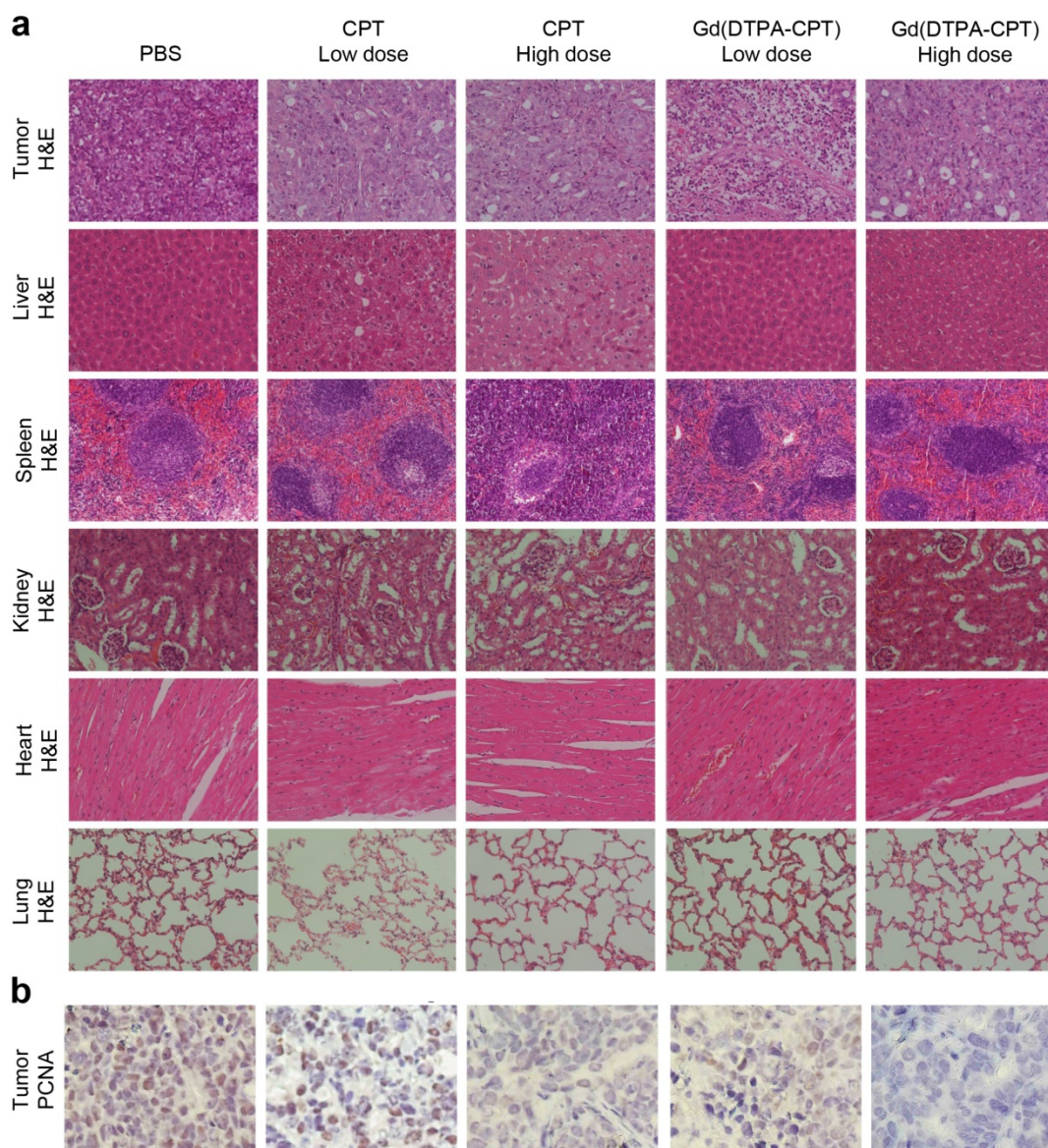


Figure 8. Histological examination and immunohistochemical analysis of tumor tissues and organs after treated with various formulations. (a) Representative histological features of tumors and organs stained with H&E. (b) Tumor sections were immune-stained with PCNA antibody to evaluate cellular proliferation (magnification $\times 400$).

The growth activities of tumor cells were further studied by immunohistochemical analysis using the PCNA staining. PCNA is a marker indicating cellular proliferation.[59] The PCNA-positive cells, which are indicated by brown staining, are observed at higher frequency in control group treated with PBS (Figure 8b). However, the percentages of PCNA-positive tumor cells treated with various drug formulations decrease significantly, especially for Gd(DTPA-CPT) nanoparticle treated group. Hence, both H&E examination and PCNA staining results corroborate the superior antitumor effect of Gd(DTPA-CPT) nanoparticles. In addition, systemic toxicities of Gd(DTPA-CPT) nanoparticles and free CPT were also evaluated by H&E staining after 27 days post-injection. H&E-stained sections of mice treated with Gd(DTPA-CPT) nanoparticles doesn't present noticeable abnormal damages in the heart, liver, spleen, kidney and lung, respectively, compared with the PBS control group (Figure 8a). The low systemic toxicity of Gd(DTPA-CPT) may be attributed to the fast clearance from body after therapy, indicating that Gd(DTPA-CPT) nanoparticles shows promising potential for clinical translation.

Discussion

The development of nano DDS has been vigorously pursued over the past decades for cancer treatment. Although conceptually very impressive, the clinical translation has been hampered by the following limitations. First, to satisfy the commercial requirements, the synthesis route should be simple and reproducible, which is propitious to increase the cost effectiveness. Second, the structure of nanopatform should be definite to minimize batch to batch variation. Third, the inherent drawback of nano DDS is the low drug loading capacity, resulting in large amount of carriers used in therapy. Fourth, high doses of carriers would result in chronic toxicity, serious inflammation and severe immunological responses during the degradation, metabolism and excretion processes. Fifth, nano DDS severely accumulate in the reticuloendothelial system, in which the hepatic processing and biliary excretion are relatively slow, increasing the risk of long-term toxicity and tissue damage.[35] These defects can't be obviated by conventional methods, which greatly limit the clinical translation of nano DDS.

Different from the design and construction of traditional stable nanoparticles, here we have developed amphiphilic small molecule based nanoparticles in equilibrium state in the blood circulation. The structure of amphiphilic small molecule is simple and definite, which facilitates tackling the commercial and regulatory challenges.

The amphiphilic small molecules such as Gd(DTPA-CPT) can self-assemble into nanoparticles in the absence of any carrier, which increases the drug loading efficiency (DLE) (the DLE of Gd(DTPA-CPT) is 39.6%) and eases the extra burden of the body. After i.v. administration, the assembled nanoparticles can accumulate in tumors through the nano-scale advantages, which is clarified by the MRI and biodistribution studies. After internalized by cancer cells, free antitumor drug CPT is released from the Gd(DTPA-CPT) nanoparticles via ester hydrolysis catalyzed by esterase in the cytoplasm. Our experimental results have demonstrated that the Gd(DTPA-CPT) nanoparticles exhibit great anticancer efficiency *in vitro* and *in vivo*. In the meantime, due to its inherent equilibrium, dissociation of the redundant Gd(DTPA-CPT) nanoparticles in blood circulation would result in effective clearance from the kidneys in the form of small molecules, which is verified by the MRI, pharmacokinetics and biodistribution results. Thus, thanks to the equilibrium shift, noncovalent-based nanoparticles exhibit excellent tumor-inhibition performance as well as low side effects and negligible chronic toxicity in the *in vivo* anticancer experiments.

Conclusion

In summary, we have developed *in vivo* renal-clearable nanoparticles, which are self-assembled from amphiphilic small molecule Gd(DTPA-CPT). The above mentioned results clearly show that Gd(DTPA-CPT) nanoparticles could accumulate in the tumor via passive targeting. After internalized by cancer cells, free CPT is released from Gd(DTPA-CPT) nanoparticles to treat cancer owing to the hydrolysis of the ester bond. After effective systemic delivery, the redundant nanoparticles in blood are dismantled into small molecules for renal clearance due to the decreased concentration and equilibrium shift, which may reduce the chronic toxicity. This assembly platform strategy could facilitate the clinical translation of small-molecule based nanoparticles and be generalizable for other small molecule based nano-delivery system to allow for multimodal and multifunctional applications.

Supplementary Material

Supplementary tables and figures.

<http://www.thno.org/v06p1703s1.pdf>

Acknowledgements

Y.M., Q.B.M. contributed equally to this work. The authors thank the National Basic Research Program (2015CB931801) and the National Natural Science Foundation of China (51473093, 21504055).

We thank Yue Su and Linzhu Zhou for *in vitro* experiments, Dali Wang and Bing Liu for *in vivo* experiments. We thank Lei Feng, Yijian Lai, Shi Xu, Yajuan Zou (Instrumental Analysis Center of Shanghai Jiao Tong University) for UPLC-3Q, ICP-MS and ICP assay. We also thank for the computing service provided from the High Performance Computing Center (HPCC) at Shanghai Jiao Tong University.

Competing Interests

The authors have declared that no competing interest exists.

References

- Peer D, Karp JM, Hong S, Farokhzad OC, Margalit R, Langer R. Nanocarriers as an emerging platform for cancer therapy. *Nat Nanotechnol.* 2007; 2: 751-60.
- Liu J, Huang W, Pang Y, Huang P, Zhu X, Zhou Y, et al. Molecular self-assembly of a homopolymer: an alternative to fabricate drug-delivery platforms for cancer therapy. *Angew Chem Int Ed.* 2011; 50: 9162-6.
- Crielaard BJ, Rijcken CJF, Quan L, Van Der Wal S, Altintas I, Van Der Pot M, et al. Glucocorticoid-loaded core-cross-linked polymeric micelles with tailorable release kinetics for targeted therapy of rheumatoid arthritis. *Angew Chem Int Ed.* 2012; 51: 7254-8.
- Hemp ST, Smith AE, Bryson JM, Allen MH, Long TE. Phosphonium-containing diblock copolymers for enhanced colloidal stability and efficient nucleic acid delivery. *Biomacromolecules.* 2012; 13: 2439-45.
- Rösler A, Vandermeulen GWM, Klok HA. Advanced drug delivery devices via self-assembly of amphiphilic block copolymers. *Adv Drug Del Rev.* 2012; 64: 270-9.
- Huang P, Wang D, Su Y, Huang W, Zhou Y, Cui D, et al. Combination of small molecule prodrug and nanodrug delivery: amphiphilic drug-drug conjugate for cancer therapy. *J Am Chem Soc.* 2014; 136: 11748-56.
- Cai K, He X, Song Z, Yin Q, Zhang Y, Uckun FM, et al. Dimeric drug polymeric nanoparticles with exceptionally high drug loading and quantitative loading efficiency. *J Am Chem Soc.* 2015; 137: 3458-61.
- Liu J, Liu W, Weitzhandler I, Bhattacharyya J, Li X, Wang J, et al. Ring-opening polymerization of prodrugs: a versatile approach to prepare well-defined drug-loaded nanoparticles. *Angew Chem Int Ed.* 2015; 54: 1002-6.
- Movassaghian S, Merkel OM, Torchilin VP. Applications of polymer micelles for imaging and drug delivery. *WIREs Nanomed Nanobiotechnol.* 2015; 7: 691-707.
- Shi Y, Van Der Meel R, Theek B, Oude Blenke E, Pieters EHE, Fens MHAM, et al. Complete regression of xenograft tumors upon targeted delivery of paclitaxel via II-II stacking stabilized polymeric micelles. *ACS Nano.* 2015; 9: 3740-52.
- Chen W, Meng F, Cheng R, Deng C, Feijen J, Zhong Z. Facile construction of dual-bioresponsive biodegradable micelles with superior extracellular stability and activated intracellular drug release. *J Control Release.* 2015; 210: 125-33.
- Kudo S, Nagasaki Y. A novel nitric oxide-based anticancer therapeutics by macrophage-targeted poly(l-arginine)-based nanoparticles. *J Control Release.* 2015; 217: 256-62.
- Yang C, Liu SQ, Venkataraman S, Gao SJ, Ke X, Chia XT, et al. Structure-directing star-shaped block copolymers: Supramolecular vesicles for the delivery of anticancer drugs. *J Control Release.* 2015; 208: 93-105.
- Kumar R, Kulkarni A, Nagesha DK, Sridhar S. In vitro evaluation of theranostic polymeric micelles for imaging and drug delivery in cancer. *Theranostics.* 2012; 2: 714-22.
- Yu H, Guo C, Feng B, Liu J, Chen X, Wang D, et al. Triple-layered pH-responsive micelleplexes loaded with siRNA and cisplatin prodrug for NF-Kappa B targeted treatment of metastatic breast cancer. *Theranostics.* 2016; 6: 14-27.
- Amstad E, Kohlbrecher J, Müller E, Schweizer T, Textor M, Reimhult E. Triggered release from liposomes through magnetic actuation of iron oxide nanoparticle containing membranes. *Nano Lett.* 2011; 11: 1664-70.
- Wang D, Tu C, Su Y, Zhang C, Greiser U, Zhu X, et al. Supramolecularly engineered phospholipids constructed by nucleobase molecular recognition: upgraded generation of phospholipids for drug delivery. *Chem Sci.* 2015; 6: 3775-87.
- Nie Y, Ji L, Ding H, Xie L, Li L, He B, et al. Cholesterol derivatives based charged liposomes for doxorubicin delivery: preparation, in vitro and in vivo characterization. *Theranostics.* 2012; 2: 1092-103.
- Lee CC, MacKay JA, Fréchet JM, Szoka FC. Designing dendrimers for biological applications. *Nat Biotechnol.* 2005; 23: 1517-26.
- Wang X, Cai X, Hu J, Shao N, Wang F, Zhang Q, et al. Glutathione-triggered "off-on" release of anticancer drugs from dendrimer-encapsulated gold nanoparticles. *J Am Chem Soc.* 2013; 135: 9805-10.
- Chen LJ, Zhao GZ, Jiang B, Sun B, Wang M, Xu L, et al. Smart stimuli-responsive spherical nanostructures constructed from supramolecular metal dendrimers via hierarchical self-assembly. *J Am Chem Soc.* 2014; 136: 5993-6001.
- Zhou Y, Huang W, Liu J, Zhu X, Yan D. Self-assembly of hyperbranched polymers and its biomedical applications. *Adv Mater.* 2010; 22: 4567-90.
- Jin H, Huang W, Zhu X, Zhou Y, Yan D. Biocompatible or biodegradable hyperbranched polymers: from self-assembly to cytomimetic applications. *Chem Soc Rev.* 2012; 41: 5986-97.
- Liu G, Zhang G, Hu J, Wang X, Zhu M, Liu S. Hyperbranched self-immolative polymers (hSIPs) for programmed payload delivery and ultrasensitive detection. *J Am Chem Soc.* 2015; 137: 11645-55.
- Wang D, Zhao T, Zhu X, Yan D, Wang W. Bioapplications of hyperbranched polymers. *Chem Soc Rev.* 2015; 44: 4023-71.
- Lim EK, Huh YM, Yang J, Lee K, Suh JS, Haam S. PH-triggered drug-releasing magnetic nanoparticles for cancer therapy guided by molecular imaging by MRI. *Adv Mater.* 2011; 23: 2436-42.
- Chen F, Hong H, Zhang Y, Valdovinos HF, Shi S, Kwon GS, et al. In vivo tumor targeting and image-guided drug delivery with antibody-conjugated, radiolabeled mesoporous silica nanoparticles. *ACS Nano.* 2013; 7: 9027-39.
- Li H, Tan LL, Jia P, Li QL, Sun YL, Zhang J, et al. Near-infrared light-responsive supramolecular nanovalve based on mesoporous silica-coated gold nanorods. *Chem Sci.* 2014; 5: 2804-8.
- Nakamura T, Sugihara F, Matsushita H, Yoshioka Y, Mizukami S, Kikuchi K. Mesoporous silica nanoparticles for ¹⁹F magnetic resonance imaging, fluorescence imaging, and drug delivery. *Chem Sci.* 2015; 6: 1986-90.
- Tsai JLL, Zou T, Liu J, Chen T, Chan AOY, Yang C, et al. Luminescent platinum(II) complexes with self-assembly and anti-cancer properties: hydrogel, pH dependent emission color and sustained-release properties under physiological conditions. *Chem Sci.* 2015; 6: 3823-30.
- Xiao Y, Hong H, Matson VZ, Javadi A, Xu W, Yang Y, et al. Gold nanorods conjugated with doxorubicin and cRGD for combined anti-cancer drug delivery and PET imaging. *Theranostics.* 2012; 2: 757-68.
- Zhang Y, Huang Y, Li S. Polymeric micelles: nanocarriers for cancer-targeted drug delivery. *AAPS PharmSciTech.* 2014; 15: 862-71.
- Qiu LY, Bae YH. Polymer architecture and drug delivery. *Pharm Res.* 2006; 23: 1-30.
- Longmire M, Choyke PL, Kobayashi H. Clearance properties of nano-sized particles and molecules as imaging agents: considerations and caveats. *Nanomedicine.* 2008; 3: 703-17.
- Feng B, LaPerle JL, Chang G, Varma MV. Renal clearance in drug discovery and development: molecular descriptors, drug transporters and disease state. *Expert Opin Drug Metab Toxicol.* 2010; 6: 939-52.
- Inoue K, Yuasa H. Molecular basis for pharmacokinetics and pharmacodynamics of methotrexate in rheumatoid arthritis therapy. *Drug Metab Pharmacokinet.* 2014; 29: 12-9.
- Garimella PD, Datta A, Romanini DW, Raymond KN, Francis MB. Multivalent, high-relaxivity MRI contrast agents using rigid cysteine-reactive gadolinium complexes. *J Am Chem Soc.* 2011; 133: 14704-9.
- Sun M, Zhang HY, Liu BW, Liu Y. Construction of a supramolecular polymer by bridged bis(permethyl-β-cyclodextrin)s with porphyrins and its highly efficient magnetic resonance imaging. *Macromolecules.* 2013; 46: 4268-75.
- Fan Q, Cheng K, Hu X, Ma X, Zhang R, Yang M, et al. Transferring biomarker into molecular probe: melanin nanoparticle as a naturally active platform for multimodality imaging. *J Am Chem Soc.* 2014; 136: 15185-94.
- Kim KS, Park W, Hu J, Bae YH, Na K. A cancer-recognizable MRI contrast agents using pH-responsive polymeric micelle. *Biomaterials.* 2014; 35: 337-43.
- Zhao Z, Fan H, Zhou G, Bai H, Liang H, Wang R, et al. Activatable fluorescence/MRI bimodal platform for tumor cell imaging via MnO₂ nanosheet-aptamer nanoprobe. *J Am Chem Soc.* 2014; 136: 11220-3.
- Caravan P, Ellison JJ, McMurry TJ, Lauffer RB. Gadolinium(III) chelates as MRI contrast agents: structure, dynamics, and applications. *Chem Rev.* 1999; 99: 2293-352.
- Jaxel C, Capranico G, Kerrigan D, Kohn KW, Pommier Y. Effect of local DNA sequence on topoisomerase I cleavage in the presence or absence of camptothecin. *J Biol Chem.* 1991; 266: 20418-23.
- Deng HP, Zhu Q, Wang DL, Zhu BS, Zhu XY. Synthesis and optical properties of GFP-mimic fluorescent polymer. *Acta Polym Sin.* 2012; 10: 1136-42.
- Li XQ, Wen HY, Dong HQ, Xue WM, Pautlett GM, Cai XJ, et al. Self-assembling nanomicelles of a novel camptothecin prodrug engineered with a redox-responsive release mechanism. *Chem Commun.* 2011; 47: 8647-9.
- Shen Y, Jin E, Zhang B, Murphy CJ, Sui M, Zhao J, et al. Prodrugs forming high drug loading multifunctional nanocapsules for intracellular cancer drug delivery. *J Am Chem Soc.* 2010; 132: 4259-65.
- Werner EJ, Datta A, Jocher CJ, Raymond KN. High-relaxivity MRI contrast agents: where coordination chemistry meets medical imaging. *Angew Chem Int Ed.* 2008; 47: 8568-80.
- Boros E, Polasek M, Zhang Z, Caravan P. Gd(DOTA)1a: a single amino acid Gd-complex as a modular tool for high relaxivity MR contrast agent development. *J Am Chem Soc.* 2012; 134: 19858-68.

49. Lee D-E, Koo H, Sun I-C, Ryu JH, Kim K, Kwon IC. Multifunctional nanoparticles for multimodal imaging and theragnosis. *Chem Soc Rev.* 2012; 41: 2656-72.
50. Lee N, Hyeon T. Designed synthesis of uniformly sized iron oxide nanoparticles for efficient magnetic resonance imaging contrast agents. *Chem Soc Rev.* 2012; 41: 2575-89.
51. Viger ML, Sankaranarayanan J, de Gracia Lux C, Chan M, Almutairi A. Collective activation of MRI agents via encapsulation and disease-triggered release. *J Am Chem Soc.* 2013; 135: 7847-50.
52. Zhu L, Wang D, Wei X, Zhu X, Li J, Tu C, et al. Multifunctional pH-sensitive superparamagnetic iron-oxide nanocomposites for targeted drug delivery and MR imaging. *J Control Release.* 2013; 169: 228-38.
53. Park JH, Gu L, von Maltzahn G, Ruoslahti E, Bhatia SN, Sailor MJ. Biodegradable luminescent porous silicon nanoparticles for *in vivo* applications. *Nat Mater.* 2009; 8: 331-6.
54. Song J, Yang X, Jacobson O, Huang P, Sun X, Lin L, et al. Ultrasmall gold nanorod vesicles with enhanced tumor accumulation and fast excretion from the body for cancer therapy. *Adv Mater.* 2015; 27: 4910-7.
55. Novakova K, Laznicek M, Rypacek F, Machova L. ¹²⁵I-labeled PLA/PEO block copolymer: biodistribution studies in rats. *J Bioact Compat Polym.* 2002; 17: 285-96.
56. Novakova K, Laznicek M, Rypacek F, Machova L. Pharmacokinetics and distribution of ¹²⁵I-PLA-*b*-PEO block copolymers in rats. *Pharm Dev Technol.* 2003; 8: 153-61.
57. Batrakova EV, Li S, Li Y, Alakhov VY, Elmquist WF, Kabanov AV. Distribution kinetics of a micelle-forming block copolymer pluronic P85. *J Control Release.* 2004; 100: 389-97.
58. Min KH, Park K, Kim YS, Bae SM, Lee S, Jo HG, et al. Hydrophobically modified glycol chitosan nanoparticles-encapsulated camptothecin enhance the drug stability and tumor targeting in cancer therapy. *J Control Release.* 2008; 127: 208-18.
59. Yu S, Zhang Y, Wang X, Zhen X, Zhang Z, Wu W, et al. Synthesis of paclitaxel-conjugated β -cyclodextrin polyrotaxane and its antitumor activity. *Angew Chem Int Ed.* 2013; 52: 7272-7.